

This document is confidential and is proprietary to the American Chemical Society and its authors. Do not copy or disclose without written permission. If you have received this item in error, notify the sender and delete all copies.

### Sensor Arrays based on Polycyclic Aromatic Hydrocarbons: Chemiresistors versus Quartz-Crystal Microbalance

Journal:	<i>ACS Applied Materials &amp; Interfaces</i>
Manuscript ID:	am-2013-03067t.R1
Manuscript Type:	Article
Date Submitted by the Author:	18-Oct-2013
Complete List of Authors:	Bachar, Nadav; Technion - Israel Institute of Technology, Liberman, Lucy; Technion - Israel Institute of Technology, Muallem, Fairouz; Technion - Israel Institute of Technology, Feng, Xinliang; Technion - Israel Institute of Technology, Mullen, Klaus; Max-Planck-Institute for Polymer Research, Haick, Hossam; Technion - Israel Institute of Technology, Department of Chemical Engineering

SCHOLARONE™  
Manuscripts

1  
2  
3 **Sensor Arrays based on Polycyclic Aromatic Hydrocarbons:**  
4  
5 **Chemiresistors vs. Quartz-Crystal Microbalance**  
6  
7

8  
9 Nadav Bachar,<sup>⊥</sup> Lucy Liberman,<sup>⊥</sup> Fairouz Muallem<sup>⊥</sup>, Xinliang Feng,<sup>§</sup>  
10 Klaus Müllen,<sup>§</sup> and Hossam Haick\*<sup>⊥</sup>  
11

12  
13  
14 <sup>⊥</sup> *The Department of Chemical Engineering and Russell Berrie Nanotechnology Institute, Technion –*  
15 *Israel Institute of Technology, Haifa 3200003, Israel*

16  
17 <sup>§</sup> *Max-Planck-Institute for Polymer Research, Postfach 3148, D-55021 Mainz, Germany*  
18  
19

20  
21 **CORRESPONDING AUTHOR: Hossam Haick**

22 Department of Chemical Engineering and Russell Berrie Nanotechnology Institute,  
23 Technion–Israel Institute of Technology, Haifa 3200003, Israel.

24 Tel: +972(4)8293087; Fax: +972-77-8871880; E-mail: [hhossam@technion.ac.il](mailto:hhossam@technion.ac.il)  
25  
26  
27  
28  
29  
30  
31  
32  
33  
34  
35  
36  
37  
38  
39  
40  
41  
42  
43  
44  
45  
46  
47  
48  
49  
50  
51  
52  
53  
54  
55  
56  
57  
58  
59  
60

**ABSTRACT**

Arrays of broadly cross-reactive sensors are key elements of smart, self-training sensing systems. Chemically sensitive resistors and quartz-crystal microbalance (QCM) sensors are attractive for sensing applications that involve the detection and classification of volatile organic compounds (VOCs) in the gas phase. Polycyclic aromatic hydrocarbon (PAH) derivatives as sensing materials can provide good sensitivity and robust selectivity towards different polar and nonpolar VOCs, while being quite tolerant to large humidity variations. Here, we present a comparative study of chemiresistor and QCM arrays based on a set of custom-designed PAH derivatives having either purely nonpolar coronas or alternating nonpolar and strongly polar side chain termination. The arrays were exposed to various concentrations of representative polar and nonpolar VOCs under extremely varying humidity conditions (5-80% RH). The sensor arrays' classification ability of VOC polarity, chemical class and compound separation was explained in terms of the sensing characteristics of the constituent sensors and their interaction with the VOCs. The results presented here contribute to the development of novel versatile and cost-effective real-world VOC sensing platforms.

**KEY WORDS:** Polycyclic Aromatic Hydrocarbon; volatile organic compound; polarity; sensor array; chemiresistor; quartz-crystal microbalance

## INTRODUCTION

Arrays of broadly cross-reactive sensors have received significant attention as key elements of smart, self-training sensing systems.<sup>1-5</sup> These arrays could meet the growing demand for rapid and flexible online detection of a wide range of chemical and biological agents in different branches of industry, homeland security,<sup>5, 6</sup> environmental monitoring,<sup>5, 7, 8</sup> and medical diagnostics<sup>1-5, 9-20</sup>. Combined with statistical algorithms, these sensor arrays can provide convenient bionics of the mammalian olfactory system for identifying complex gas samples, without the necessity of identifying their separate ingredients.<sup>1-5</sup> In this configuration, every sensing element responds to all or to part of the chemical compounds in the gas sample. Odor-specific response patterns are then established by applying pattern recognition- and classification algorithms.<sup>21, 22</sup> A sensor array can be trained for the selective detection of a specific odor by repeated exposure. Thereafter, unknown samples can be identified by comparison with the patterns stored in a database.

When using this strategy, the sensing platforms and sensing materials must be prudently chosen to ensure sufficient detection limits and dynamic ranges for the chemical compounds that cause the odors of interest.<sup>1, 3</sup> Additionally, it has to be chosen with tolerance to variable background parameters that typically occur in real-world applications.<sup>1, 3, 5</sup> For example, varying levels of ambient humidity usually alter the sensing signals, leading to a decrease in sensitivity and selectivity towards the desired compound(s).<sup>12, 23</sup> The implementation of the sensors should be simple and cost-effective enough to be economically viable for real-world applications. Sensors with electronic and electro-acoustic transduction mechanisms, such as chemically sensitive resistors<sup>24-33</sup> and quartz-crystal microbalance (QCM) sensors<sup>34-36</sup> are among the most attractive and widespread elements for sensing applications that involve the detection and classification of volatile organic compounds (VOCs) in the gas phase.<sup>9, 11, 13, 16, 19, 20, 24, 37</sup>

1  
2  
3 Recently, we have shown that polycyclic aromatic hydrocarbon (PAH) derivatives as  
4 sensing materials in chemiresistors, field effect transistors or QCM sensors can provide good  
5 sensitivity and robust selectivity towards different polar and nonpolar VOCs, while being  
6 highly tolerant even to drastic humidity variations.<sup>11, 33, 34, 38-40</sup> For example, we have shown  
7 that a bilayer structure with a quasi 2D network of single wall carbon nanotubes (RN-  
8 SWCNTs) as an under-layer and a micron-thick PAH film as an overcoat, can provide  
9 excellent detection and classification between polar and nonpolar VOCs, both in dry  
10 atmospheres with ~ 5% relative humidity (RH) and in almost fully humidified atmospheres  
11 (~80% RH).<sup>33, 34, 38</sup> Electrical current flowing through the structure favors the low resistance  
12 RN-SWCNTs, and, therefore, the PAH films serve mainly as an adsorption phase for the  
13 targeted VOCs.<sup>33, 38-40</sup> Nevertheless, the interaction between the VOCs the chemical/physical  
14 properties of the PAH sensing materials, as well as their incorporation into arrays of  
15 chemiresistors and QCM sensors still need further exploration.

16  
17  
18  
19  
20  
21  
22  
23  
24  
25  
26  
27  
28  
29  
30  
31  
32 Here, we present a comparative study of the sensing performance of six custom-  
33 designed PAH derivatives having purely nonpolar alkyl side chains or alternating nonpolar  
34 and strongly polar side chain termination. The PAH layers were applied as sensing elements  
35 in PAH-functionalized RN-SWCNT chemiresistors and in PAH-coated QCM sensors. The  
36 sensing responses to representative polar and nonpolar VOCs from the families of alcohols,  
37 alkanes, ethers and aromatics were studied at a range of concentrations and under extremely  
38 varying humidity conditions, from dry to almost fully humidified atmospheres. The  
39 classification ability of VOCs polarity, chemical class and compound separation was  
40 determined for chemiresistor arrays and QCM sensor arrays incorporating the same set of  
41 sensing materials and was explained in terms of the sensing characteristics of the constituent  
42 sensors. Sub-arrays containing either PAH with nonpolar alkyl side chains or PAHs  
43  
44  
45  
46  
47  
48  
49  
50  
51  
52  
53  
54  
55  
56  
57  
58  
59  
60

1  
2  
3 containing alternating nonpolar and strongly polar end groups were tested and compared in  
4  
5 order to gain better insight into the interaction between VOCs and PAH sensing elements.  
6  
7

## 8 9 10 **EXPERIMENTAL SECTION**

### 11 **Device preparation**

12  
13 The properties (core and side-chains) and the widely modified molecular structures of the six  
14  
15 PAH derivatives that were used in this study are listed in Table 1. The cores are hydrophobic  
16  
17 mesogens, either aromatic cores with a carbon number of 42 (PAH-B, PAH-C), semi-triangle  
18  
19 shaped aromatic cores with a carbon number of 48 (PAH-3, PAH-4 and PAH-5), or a triangle-  
20  
21 shaped core with a carbon number of 60 (PAH-A). The side chains are different straight and  
22  
23 branched alkyl chains that are in part terminated with functional substituents, such as ester  
24  
25 (PAH-3) and carboxylic acid (for PAH-4 and PAH-5). The synthesis of the three PAH  
26  
27 derivatives with nonpolar side-chains (PAH-A, PAH-B, PAH-C) has been described in Refs.  
28  
29 41, 42. The synthesis of the three PAH derivatives with alternating nonpolar and strongly  
30  
31 polar side-chains (PAH-3, PAH-4, and PAH-5) will be described elsewhere.  $10^{-3}$  M PAH  
32  
33 solutions were prepared in toluene (PAH-A; PAH-C; and PAH-3), in tetrahydrofuran (PAH-4;  
34  
35 and PAH-5) or in xylene (PAH-B). PAH molecules easily self-assemble into long molecular  
36  
37 stacks with a large, electron rich, semiconducting core, providing good charge carrier  
38  
39 transport along the molecular stacking direction and a relatively insulating periphery.<sup>41, 43-45</sup>  
40  
41 The molecular PAH columns typically form micrometer sized, and sponge-like 3D structures  
42  
43 with a high surface-to-volume ratio.<sup>33, 39, 40</sup>  
44  
45

46  
47  
48  
49 Mass-sensitive sensors were prepared by drop-casting 2 $\mu$ L of PAH solution on gold-  
50  
51 plated Quartz Crystal Microbalance (QCM) resonators.<sup>33, 34, 39, 40, 46</sup> The devices were dried  
52  
53 for 30 min under ambient conditions, then placed into a desiccator and kept overnight under  
54  
55 vacuum. Chemiresistors were prepared from hybrid layers of quasi-2D random networks of  
56  
57  
58  
59  
60

1  
2  
3 single walled carbon nanotubes (RN-SWCNTs) that were capped with micron-thick PAH  
4 layers, as described previously.<sup>33, 39, 40</sup> Briefly, 10 pairs of circular interdigitated (ID)  
5 electrodes (outer diameter: 3000  $\mu\text{m}$ ; electrode spacing & electrode width: 25  $\mu\text{m}$ ) were  
6 deposited on substrates (*p-type* Si (100) with a 1 $\mu\text{m}$  thermal oxide), by electron-beam  
7 evaporation of 25nm/200nm Ti/Au, using conventional photolithography. Electrically  
8 continuous RN-SWCNTs were prepared by drop-casting 0.02%wt SWCNT solution (ARRY  
9 International LTD, Germany; average diameter: 1.5 nm; average length: 7  $\mu\text{m}$ ; ~30%  
10 metallic/70% semiconducting) in dimethylformamide (DMF; Sigma Aldrich Ltd.; >98%  
11 purity) onto the ID electrodes. The RN-SWCNT devices were dried overnight in a vacuum  
12 oven and subsequently coated with chemiresistive PAH layers by drop-casting 2 $\mu\text{L}$  of  
13 solution. The PAH/RN-SWCNT chemiresistors were dried under ambient conditions for 30  
14 min, subsequently placed in a desiccator and kept under vacuum overnight. The PAH  
15 deposition process was twice repeated to obtain nearly continuous PAH cap-layers, as in the  
16 QCM devices. The morphology of the PAH films in both chemiresistors and QCM devices  
17 were similar to each the other and were similar to those presented and discussed by us in an  
18 earlier report.<sup>38</sup>

### 40 **Description of the Sensor Arrays**

41  
42 Two sensor arrays were studied. The constituent sensors of these arrays are summarized in the  
43 Table S1 in the supporting information. Array 1 incorporated six PAH/RN-SWCNT  
44 chemiresistors. Array 2 consisted of six PAH-functionalized mass sensitive QCM devices.  
45 Each of the six constituent sensors was functionalized with one of the six PAH derivatives  
46 listed in Table 1; both arrays included all of the six available PAH derivatives. The PAH  
47 derivatives formed two groups (*see* Table 1): (i) PAH-A,B&C had different poly-aromatic  
48 cores and different nonpolar hydrophobic alkyl side-chains; (ii) PAH-3,4&5 had the same  
49  
50  
51  
52  
53  
54  
55  
56  
57  
58  
59  
60

1  
2  
3 semi-triangular poly-aromatic cores (carbon number: 48) and different side chains: alternating  
4  
5 nonpolar hydrophobic alkyl side-chains and strongly polar hydrophilic side-chains terminated  
6  
7 with different polar functional substituents.  
8

9  
10 Array 1 was characterized by electrical measurements before and after exposure to a  
11 series of polar and nonpolar VOCs (*see* Table 2) at various concentrations and under different  
12 relative humidity (RH) backgrounds. Array 2 was characterized by mass absorption  
13 measurements under the same exposure conditions (*see* below).  
14  
15  
16  
17  
18  
19

### 20 21 **Exposure to VOC Vapors**

22  
23 Table 2 lists the polar and nonpolar VOCs that were used in this study: DI-water from a  
24 commercial water purification system (Easypure II); 1-decanol, dibutylether and mesitylene  
25 (all from Sigma-Aldrich Ltd.); 1-hexanol and 1-octanol (from Fluka Analytical Ltd), ethanol  
26 and *n*-hexane (from Frutarom Ltd.); *n*-decane (from Arcos Organics); *n*-octane (from Merck  
27 Schuchardt Ltd). Purity of all VOCs >99%.  
28  
29  
30  
31  
32  
33

34 VOC vapors were supplied to the sensors using an automated, computer-controlled  
35 flow system, capable of regulating the VOC concentrations and the background humidity  
36 level. Oil-free, purified air from a compressed air source (baseline RH: 5.0±0.2%; organic  
37 contamination determined by a commercial PID ppbRAE 3000 detector < 0.3 ppm), was used  
38 as a carrier gas and as a reference gas. The VOC or water vapours were produced by bubbling  
39 air through liquid VOCs in glass bubblers. Saturated VOC vapors were carried out from the  
40 side arm of the bubbler and diluted with a carrier gas at a flow rate of 0.5–5.0 L/min. By  
41 regulating the flow between the saturated VOC vapor and the gas carrier, various  
42 concentrations ( $p_a/p_o=0.05$  to 0.2, where  $p_a$  stands for the partial pressure of the VOC and  $p_o$   
43 stands for the saturated vapor pressure at 21 °C)<sup>47</sup> were achieved. The background relative  
44 humidity (RH; *i.e.* the ratio of the partial pressure of water vapor in the air–water mixture to  
45  
46  
47  
48  
49  
50  
51  
52  
53  
54  
55  
56  
57  
58  
59  
60



1  
2  
3 the saturated vapor pressure of water at the prescribed temperature) of the carrier gas was  
4 regulated by a deliberate mixing of dry air ( $5.0 \pm 0.2\%$  RH) and fully humidified air (100%  
5 RH) coming out of the water bubbler) flows. Three main background RH were used: 5%,  
6  
7 40% and 80% RH.  
8  
9

10  
11 Sensing experiments were performed continuously, using 9 subsequent exposure  
12 cycles in a flow mode with incremental increase of the VOC concentration: (i) exposure to  
13 synthetic dry air flow with RH=5% for 10 min; (ii) exposure to VOC vapor at  $p_a/p_o=0.05$  at a  
14 fixed background RH for 10 min; (iii) purging the chamber with dry air for 10 min; (iv)  
15 exposure to VOC vapor at  $p_a/p_o=0.10$  (fixed RH background) for 10 min; (v) purging the  
16 chamber with dry air for 10 min; (vi) exposure to VOC vapor at  $p_a/p_o=0.16$  (fixed RH  
17 background) for 10 min; (vii) purging the chamber with dry air for 10 min; (viii) exposure to  
18 VOC vapor at  $p_a/p_o=0.2$  (fixed RH background) for 10 min; (ix) purging the chamber with dry  
19 air for 10 min.<sup>47</sup> These 9 exposure cycles were performed for three fixed background RH  
20 levels of 5%, 40% and 80%.<sup>48</sup> Every experiment was run twice to test reproducibility. Array 1  
21 was characterized by electrical measurements during the multi-cycle exposures to a series of  
22 polar and nonpolar VOCs (see below). Array 2 was characterized continuously by mass  
23 absorption measurements under the same exposure conditions (see below).  
24  
25  
26  
27  
28  
29  
30  
31  
32  
33  
34  
35  
36  
37  
38  
39  
40  
41  
42

### 43 **Electrical Measurements**

44  
45 The six PAH/ RN-SWCNT chemiresistors were integrated into TO5 holders by wire bonding.  
46  
47 The bonded devices were then mounted on a custom circuit board with twenty separated  
48 sensor sites and were horizontally inserted into a 350 ml stainless steel exposure chamber.  
49  
50 Both gas inlet and outlet were parallel to the sensors stage in the chamber. The changes in  
51 resistance under VOC exposure were measured using the Agilent multifunction switch 34980.  
52  
53  
54  
55  
56 A Stanford Research System SR830 DSP lock-in amplifier controlled by an IEEE488 bus  
57  
58  
59  
60

1  
2  
3 was used to supply the AC voltage signal (0.2 V at 1 kHz) and to measure the corresponding  
4  
5 current ( $<10\mu\text{A}$  in the studied devices). The entire system was controlled by a custom  
6  
7 Labview program. The relative resistance change,  $\Delta R/R_b$ , was determined from the measured  
8  
9 data (see supporting information, Figure S1b), where  $\Delta R$  is the resistance change ( $R-R_b$ ) of the  
10  
11 film upon exposure to VOC and  $R_b$  is the films baseline resistance in dry air prior to the  
12  
13 exposure.  
14  
15  
16  
17  
18

### 19 **Mass Absorption Measurements**

20  
21 QCM sensors are piezoelectric mass-sensing devices that can detect very small mass changes,  
22  
23 down to a fraction of a monolayer or a single atomic layer. A QCM sensor measures the  
24  
25 change in frequency ( $\delta f$ ) of a quartz crystal resonator resulting from the addition or removal  
26  
27 of a small mass ( $\Delta m$ ) at the surface of the acoustic resonator.  $\Delta m$  can be determined from  $\delta f$   
28  
29 using the Sauerbrey's equation,  $\Delta m = -C_f A \cdot \delta f$ ;  $C_f$ : mass sensitivity (here:  $1.104 \text{ ng}\cdot\text{cm}^{-2}\cdot\text{Hz}^{-1}$ );  
30  
31  $A$ : active area of the QCM resonator (here:  $0.2 \text{ cm}^2$ ). The frequency shifts ( $\delta f$ ), before  
32  
33 and after exposure to VOC vapors were recorded simultaneously for the six PAH-QCM  
34  
35 sensors, using a LibraNose 2.1 system (Technobiochip, Elba Island, Italy). This QCM system  
36  
37 incorporates a stainless steel exposure chamber with eight QCM mounts that are located in  
38  
39 parallel to gas flow, an internal micro-pump and a micro-electric valve that conveys the VOC  
40  
41 vapors to the exposure chamber with the sensors. The gas inlet entered from the bottom of the  
42  
43 chamber and the outlet stream exited from its top. The relative frequency shift,  $\Delta f/f_{ob}$ , was  
44  
45 determined from the measured data (see supporting information, Figure S1a), where  $\Delta f$  is the  
46  
47 frequency change ( $f-f_b$ ) of the device upon exposure to VOC and  $f_b$  is the baseline frequency.  
48  
49 The baseline normalizations were carried out in order to remove any variability due to the use  
50  
51 of different film thickness and/or mass between experiments on a given type of film. The  
52  
53 results were given as relative mass change,  $\Delta m/m_b$ .  
54  
55  
56  
57  
58  
59  
60

## Statistical Analysis of the Sensors Array Output

Collective patterns were derived from the output of the sensor arrays, using principle component analysis (PCA) and discriminant factor analysis (DFA).<sup>49</sup> PCA is a non-supervised linear multivariate analysis method which reduces the complexity of the data-set, from initial  $n$ -dimensional space to a few dimensions. This is done using a linear combination of the original measured variables resulting in new uncorrelated (orthogonal) variables called principle components (PCs). These PCs allow preserving the data-set inherent structure while its resulting variance is maximized. PCA is performed with no information on the classification of samples and it is based solely on the intrinsic variance of the original data set. On the other hand, DFA is a supervised linear multivariate analysis method that is supplied with the classification information regarding every measurement in the training set. DFA finds new orthogonal axes (canonical variables) as a linear combination of the input variables, computing these factors for minimizing the intra-class variance while maximizing the inter-class variance. The classification accuracy is determined by leave-one-out cross-validation. Given  $n$  measurements, DFA is computed  $n$  times using  $n-1$  training vectors. The left out vector (*i.e.* the validation vector that is invisible during the training phase) is then projected onto the DFA model, producing a classification result. The classification accuracy is estimated as the averaged performance over the  $n$  tests. The statistical tests were performed by SAS JMP, ver. 9.

## RESULTS AND DISCUSSION

### Response Characteristics of PAH/RN-SWCNT Chemiresistors and PAH-QCM

Each of the twelve tested sensors in array 1 & array 2 (*see* supporting information, Table S1) responded rapidly and reproducibly to the exposure of the polar and nonpolar VOCs that are listed in Table 2, at the studied concentrations between  $p_a/p_o=0.05$  and  $p_a/p_o=0.2$ , and under

1  
2  
3 different RH background levels of 5%, 40% and 80%. All signals were well above the  
4  
5 detection- and quantification limits of the sensors. Two representative examples of the  
6  
7 recorded net sensing responses (of the PAH-4 QCM sensor and the PAH-4/RN-SWCNT  
8  
9 chemiresistor during one complete hexane cycle at 5% RH), are given in the supporting  
10  
11 information, Figure S1.  
12

13  
14 Negative frequency shifts were observed for all the PAH-coated QCM sensors upon  
15  
16 exposure to the VOCs, corresponding to an increase in the PAH films' mass. This mass  
17  
18 increase could be due to (i) dissolution of VOC molecules into the PAH layer, and/or (ii)  
19  
20 accumulation of VOC molecules on top of the PAH layer surface. Positive resistance shifts  
21  
22 were observed for all six PAH/RN-SWCNT chemiresistors, corresponding to a decrease in  
23  
24 the PAH films' conductivity. When switching off the vapor supply and purging the exposure  
25  
26 chamber with dry air, the QCM sensors returned rapidly to their baseline frequencies. The  
27  
28 baseline shifts were negligible. The chemiresistors showed a small and constant drift in  
29  
30 baseline resistance with time. The changes in the electrical resistance and resonant frequency  
31  
32 that can be observed in Figure 1S of the supporting information were caused exclusively by  
33  
34 exposure to the VOC/water vapors since the total flow rate, RH level ( $\pm 3\%$ ) and temperature  
35  
36 ( $\pm 2$  °C) were maintained constant throughout the experiments. Evidently, as the VOC  
37  
38 concentration increased, the responses, in their absolute value, increased as well. For the sake  
39  
40 of comparative analysis, we extracted the relative responses in the form of  $\Delta R/R_b$  and  $\Delta m/m_b$   
41  
42 from the measured time-dependent sensing responses of the chemiresistors and of the QCM  
43  
44 sensors, respectively.  
45  
46  
47  
48

49  
50 The sensing properties of PAH-films are primarily determined by the properties of the  
51  
52 side chains of the PAH molecules. Figure 1 compares the performance as sensing matrix in  
53  
54 chemiresistors and QCM devices of a PAH derivative with only nonpolar side-chains to that  
55  
56 of a PAH derivative having strongly polar outer termination. PAH-A with branched alkyl  
57  
58  
59  
60

1  
2  
3 chains was taken as a representative example of the former, and PAH-4 with alternating  
4  
5 branched alkyl and carboxyl terminated phenyl side-chains served as representative example  
6  
7 for the latter.  
8

9  
10 Figures 1 (a&b) show  $\Delta R/R_b$  of the PAH-A/RN-SWCNT and PAH-4/RN-SWCNT  
11 chemiresistors vs. the VOC concentration ( $p_a/p_o$ ) for all studied VOCs at 5% background RH.  
12  
13 Figures 1 (c&d) show the concentration dependence of  $\Delta m/m_b$  for QCM devices incorporating  
14  
15 the same PAH films under identical conditions. It was observed that for all tested VOCs both  
16  
17  $R/R_b$  and  $\Delta m/m_b$  increased in good approximation linear with increasing VOC concentrations  
18  
19 ( $R^2 > 0.9$ ) within the tested range of concentrations ( $p_a/p_o=0.05-0.2$ ). The chemiresistors  
20  
21 exhibit good VOC separation of similar magnitude over the entire range of compositions for  
22  
23 both PAH molecules, while the signals of the QCM devices overlapped strongly at  
24  
25  $p_a/p_o=0.05$ , but fanned out at higher concentrations. This trend was more pronounced for  
26  
27 PAH-A than for PAH-4.  
28  
29  
30  
31

32 Both PAH-A and PAH-4 showed lower uptake of the polar VOCs than of the nonpolar  
33  
34 ones (see Figure 1 c&d); the mass uptake of PAH-A was almost negligible and smaller than  
35  
36 that of PAH-4, in agreement with our earlier studies.<sup>34</sup> However, the relatively small mass  
37  
38 changes after polar VOC exposure were sufficient to produce significant changes in the  
39  
40 electrical resistance both for PAH-A and PAH-4. In contrast, the nonpolar VOCs yielded  
41  
42 significant mass uptakes correlated with relatively low changes in  $\Delta R/R_b$  (see Figure 1 a&b).  
43  
44 Remarkably, the uptake of polar molecules and water was smaller for PAH-A than for PAH-  
45  
46 4, while their resistance responses were similar. Hence, the difference in sensing performance  
47  
48 between the QCM devices and the chemiresistors must be more pronounced for the PAH-A  
49  
50 macromolecule with the nonpolar side-chains than for PAH-4 with mixed nonpolar and polar  
51  
52 side chains. This could be observed clearly when plotting  $\Delta R/R_b$  vs.  $\Delta m/m_b$  (see Figure 1 e&f).  
53  
54 For PAH-A, the curves for the polar VOCs had a very steep increase of  $\Delta R/R_b$  within a very  
55  
56  
57  
58  
59  
60

1  
2  
3 small  $\Delta m/m_b$  interval and remained close to the  $\Delta R/R_b$  -axis, while the curves for nonpolar  
4  
5 VOCs were shallow and displayed only a moderate increase of  $\Delta R/R_b$  with increasing mass  
6  
7 uptake. PAH-4 showed a similar but considerably less pronounced trend.  
8  
9

10 The change in the slopes of  $\Delta R/R_b$  vs.  $\Delta m/m_b$  was illustrated in Figures 1 g&h by  
11  
12 plotting their ratio against the VOC concentration for PAH-A and PAH-4, respectively. For  
13  
14 the nonpolar VOCs, the ratios of  $\Delta R/R_b$  and  $\Delta m/m_b$  were almost constant and close to 1 over  
15  
16 the entire range of VOC concentrations. This trend was observed both for PAH-A and PAH-4.  
17  
18 The good agreement between mass uptake and resistance response could possibly indicate the  
19  
20 following: the nonpolar VOCs causing the observed mass increase of the PAH layer were  
21  
22 mostly dissolved into the layer (and did hardly accumulate on top of the layer surface), thus  
23  
24 causing a corresponding volume change or fractional swelling of the PAH film, which in turn  
25  
26 disrupted the underlying RN-SWCNTs, thus leading to the observed proportional increase in  
27  
28 the electrical resistance. However, further investigations of the morphological changes of the  
29  
30 PAH layer under VOC exposure would be necessary before far-reaching conclusion can be  
31  
32 drawn. In contrast, a strong discrepancy was observed for polar VOCs at low concentrations  
33  
34 between resistance response and mass uptake. This trend was most pronounced for all the  
35  
36 polar VOCs (except for water) at the lowest VOC concentration of  $p_a/p_o=0.05$ . Again, the  
37  
38 discrepancies were more obvious for PAH-A ( $\Delta R/R_b$  up to two orders of magnitude higher  
39  
40 than  $\Delta m/m_b$ ) than for PAH-4 (about 1 order of magnitude difference). The discrepancies  
41  
42 decreased monotonically, in a linear way, for increasing VOC concentrations, but still  
43  
44 remained higher than for the nonpolar VOCs over the entire range of concentrations. We  
45  
46 propose the following educated guess about the possible underlying physical mechanism:  
47  
48 only part of the polar VOCs could be dissolved into the PAH layer, while the rest remained on  
49  
50 the surface, forming VOC accumulation layer.<sup>50, 51</sup> It would be reasonable to assume that at  
51  
52 low VOC concentrations the proportion of VOC molecules entering the PAH layer would be  
53  
54  
55  
56  
57  
58  
59  
60

1  
2  
3 higher than at higher concentrations, due to saturation.<sup>52-54</sup> However, as mentioned before,  
4  
5 detailed morphological studies under VOC exposure would be necessary to confirm this  
6  
7 hypothesis. For pure water vapor at concentrations of  $p_a/p_o=0.05-0.2$ , the relative resistance  
8  
9 response  $\Delta R/R_b$  of PAH-A was about 30 times higher than relative mass uptake  $\Delta m/m_b$ , while  
10  
11  $\Delta R/R_b$  of PAH-4 was only about 5 times higher than  $\Delta m/m_b$ . Clearly, the sensing mechanism  
12  
13 for polar VOCs is more complex than for nonpolar VOCs and most probably results from an  
14  
15 interplay of different physical mechanisms for the interaction of the polar VOCs with the  
16  
17 PAH layer that are related to charge exchange and/or dielectric effects. This may include, but  
18  
19 are not limited to: (a) a decrease in the electron hopping rate in the film caused by an increase  
20  
21 in the dielectric constant of the film's medium<sup>50</sup> due to the incorporation of polar molecules  
22  
23 having a high dielectric constant than the PAH host layer (*see* Table 2); and/or (b) a reduction  
24  
25 in the concentration of the charge carriers and, hence, in the conductivity, of the PAH layer,  
26  
27 probably due to electron withdrawal by the electronegative oxygen atom in the hydroxyl  
28  
29 group attached to the saturated carbon in the polar molecule.<sup>55</sup>  
30  
31  
32  
33

34 Similar trends were observed for all six PAH derivatives, both as chemiresistors and  
35  
36 as QCM sensors, irrespective of the humidity background levels. The heat-map representation  
37  
38 in Figure 2 summarizes the relative resistance changes for the six studied PAH derivatives to  
39  
40 polar and nonpolar VOCs at concentrations between  $p_a/p_o = 0.05$  and  $p_a/p_o = 0.2$  and under  
41  
42 low (5%), intermediate (40%) and high (80%) background RH levels. The corresponding  
43  
44 relative mass changes are summarized in Figure 3. We assume that the sensing of polar and  
45  
46 nonpolar VOCs by the PAH films is related to molecular interactions such as dipole  
47  
48 interactions and van der Waals forces between the VOCs and PAH macromolecules, as well  
49  
50 as to the film's microstructure. At the molecular level, we assume parameters like core size  
51  
52 and shape, conjunction length, side chain nature and length and intermolecular forces (such as  
53  
54 hydrogen bonding,<sup>46, 56</sup> van der Waals and aromatic/ $\pi$ -stacking<sup>57</sup>) can dominate individually or  
55  
56  
57  
58  
59  
60

1  
2  
3 cooperatively to establish the organization of the system, thus may influence the charge  
4 transport. At the macrostructure level, we assume that parameters like film morphology,  
5 distribution of delocalized hopping states and density and height of grain boundary barrier<sup>58</sup>  
6 may also affect the conductivity. The interactions between VOCs and sensing film most likely  
7 modulate one or more of these parameters, thus regulating the current density through the  
8 film.  
9  
10  
11  
12  
13  
14  
15

16 The following observations emerged from a comprehensive comparative analysis of  
17 the sensing signals:  
18  
19

- 20  
21 (i) The responses of all chemiresistors and QCM sensors increased systematically as  
22 higher VOC concentrations were introduced. The increase of the sensing response  
23 was in good approximation proportional (linear) to the increasing VOC  
24 concentration.  
25  
26  
27  
28  
29 (ii) All PAH/RN-SWCNTs chemiresistors exhibited a higher resistance increase to  
30 ethanol than to the other VOCs. Among the nonpolar VOCs, the highest resistance  
31 increase was observed for decane.  
32  
33  
34  
35  
36 (iii) All PAH-coated QCM sensors showed the highest mass increase when exposed to  
37 the aromatic compound mesitylene. Indeed, mesitylene can act as a solvent for the  
38 PAH macromolecules. It is reasonable to assume that aromatic-aromatic  
39 interactions and/or van der Waals forces between the fused benzene rings in the  
40 PAH cores and those of the mesitylene occur that cause the enhanced mass uptake.  
41  
42  
43  
44  
45  
46  
47 (iv) In most cases the PAH-A,B&C/RN-SWCNTs chemiresistors, which possess only  
48 hydrophobic alkyl side-chains, showed lower resistance increases than the PAH-  
49 3,4&5/RN-SWCNTs, which possess alternating hydrophobic alkyl side-chains and  
50 hydrophilic side-chains terminated with different polar functional substituents. The  
51 same was observed for the PAH-coated QCM sensors.  
52  
53  
54  
55  
56  
57  
58  
59  
60



- 1  
2  
3 (v) In all PAH/QCM sensors the mass adsorption of nonpolar VOCs was higher than  
4 that of the polar VOCs, while in most PAH/RN-SWCNTs sensors the polar VOCs  
5 exhibited higher increases in resistance than the nonpolar VOCs, with the exception  
6 of decane.  
7  
8  
9  
10  
11 (vi) One of the most crucial practical issues in the gas sensing field is the influence of  
12 the humidity on the sensing parameters. Many studies have assessed the response  
13 of sensors to different VOCs, using dry nitrogen as the carrier gas. However, most  
14 practical gas sensing applications involve operation under atmospheric conditions  
15 with moderate to high humidity back grounds. Here we have studied and compared  
16 the performance of the tested PAH-based sensors in dry air (~5% RH) and in  
17 humidified air (~40% and ~80% RH). All chemiresistors showed a clear increase in  
18 resistance when the background RH levels were increased, while the VOC  
19 concentration remained the same (*see* Figure 2). Most resistance responses to  
20 VOCs diluted in 80% RH were higher than the response to the same VOCs at 5%  
21 RH, as illustrated by the drastic change of the response patterns in the heat-maps in  
22 Figure 2. For example, all PAH/RN-SWCNTs exhibited high responses upon  
23 exposure to ethanol, which became more substantial than 80% RH. Interestingly, as  
24 the RH background increased, the resistance responses to the nonpolar VOCs  
25 increased stronger than those of the polar VOCs (excluding mesitylene, which for  
26 most PAH films showed the opposite trend).  
27  
28  
29  
30  
31  
32  
33  
34  
35  
36  
37  
38  
39  
40  
41  
42  
43  
44  
45  
46  
47 (vii) In contrast, the QCM sensors gave only very low mass uptakes of water (<0.3%),  
48 even at fractions of saturated VOC vapor pressure up to 20%. In general, the PAH-  
49 coated QCM sensors did show a small increase in response to a specific VOC at a  
50 set concentration after a higher humidity background was introduced. However, the  
51 heat-maps in Figure 3 reveal that the response patterns of the QCM sensors were  
52  
53  
54  
55  
56  
57  
58  
59  
60

1  
2  
3 not dramatically affected by the drastic increase in the RH background level from  
4  
5 5% to 80%. The only exception was the performance of the PAH-B QCM sensor in  
6  
7 an atmosphere of 80% background RH.  
8  
9

### 10 11 **Performance of Cross-reactive Sensors Arrays**

12  
13 The discriminative power of the PAH/RN-SWCNT chemiresistor array (Array 1; *see*  
14 supporting information, Table S1) and the PAH-QCM sensor array (Array 2) under different  
15  
16 RH background levels was tested and compared by means of collective statistical treatment of  
17  
18 the sensing responses of the constituent sensors, using both non-supervised (*i.e.*, PCA) and  
19  
20 supervised (*i.e.*, DFA) linear multivariate data analysis methods (*see* Experimental Section).  
21  
22 Initially, PCA was used to remove the redundancy of variables and to depict representative  
23  
24 maps of the data obtained from both sensor arrays. This is achieved using a linear  
25  
26 combination of the original measured variables (*i.e.*,  $\Delta R/R_b$  for array 1 and  $\Delta m/m_b$  for array 2),  
27  
28 resulting in new uncorrelated variables called principle components (PCs). These PCs allow  
29  
30 the reduction of the data dimensionality, facilitating its visualization while retaining as much  
31  
32 information as possible.  
33  
34  
35  
36  
37

38  
39 The main panels of Figures 4 (a&b) show PCA plots that depict the separation  
40  
41 between all nine VOCs examined in the study (*see* Table 2) at  $p_a/p_o = 0.05$  and  $0.2$  and RH=5-  
42  
43 80%, using arrays 1 and 2, respectively. In the large panel of Figure 4a, it can be seen that  
44  
45 PC1 (63.3%), PC2 (22.8%) and PC3 (5.8%) account for 91.9% of the total variance. In the  
46  
47 large panel of Figure 4b, it can be seen that PC1 (76.6%), PC2 (15.3%) and PC3 (5.5%)  
48  
49 account for 97.4% of the total variance. Although it is rather difficult to observe clear clusters  
50  
51 and trends in these figures, the separated PCA plots for the three RH levels provide better  
52  
53 visualization of the data-set. The side panels of Figure 4a shows that the six PAH-  
54  
55 functionalized RN-SWCNT chemiresistors in array 1 effectively differentiate between the  
56  
57  
58  
59  
60

1  
2  
3 various VOCs under 5% RH background environment. As seen in the PCA panel at 5% RH,  
4 the data points of the polar VOCs (*i.e.*, decanol, octanol, hexanol and ethanol; presented as  
5 blue and green hollow triangles) were rather spread over the top-right quarter of the plot.  
6  
7 From the same panel, it can be seen also that the points of nonpolar VOC data (*i.e.*, decane,  
8 octane, hexane, dibutylether and mesitylene; presented as full orange, violet and reddish  
9 shapes) are scattered over (or in proximity) to the bottom-left quarter of the plot. However,  
10 increasing the RH background levels to 40% and 80% RH blurs this separation slightly.  
11  
12  
13  
14  
15  
16  
17

18 The PCA plots ascribed to the six PAH-coated QCM sensors in array 2 (*see* side  
19 panels of Figure 4b) show that the data points of the polar VOCs under atmosphere of 5% RH  
20 are concentrated in the bottom-left quarter of the plot. Additionally, the same plot shows that  
21 the nonpolar data points are scattered mostly in the right hemisphere of the plot. While slight  
22 overlap of data points is presented under atmospheres of 40% and 80% RH, their general  
23 distribution does not change compared to that obtained under 5% RH background.  
24  
25  
26  
27  
28  
29  
30

31 Interestingly, both array 1 and array 2 exhibit an increase in the PC1 values upon increasing  
32 the concentration from  $p_a/p_o=0.05$  to  $p_a/p_o=0.2$  for all examined VOCs. Note that the PC  
33 values calculated for each VOC in the separate panels were not identical to the PC values  
34 presented in the main figure, because the input data for the models was different.  
35  
36  
37  
38  
39

40 In order to extensively study and evaluate the classification abilities of the two arrays  
41 we employed several DFA models on the data-set. The main panel of Figure 5a shows how  
42 array 1 successfully separated the entire group of polar VOCs from the entire group of  
43 nonpolar VOCs (*cf.* Table 2) at mixed concentrations between  $p_a/p_o = 0.05$  and 0.2, and under  
44 extremely variable RH background levels between 5% and 80% RH. The side panels provide  
45 separate DFA models for the three RH background levels. Note the CV1 values calculated for  
46 each VOC in the separate DFA models were not identical with the CV1 values of the same  
47 VOC at the corresponding RH levels in the overall model, because the input data for the  
48  
49  
50  
51  
52  
53  
54  
55  
56  
57  
58  
59  
60

1  
2  
3 models was different. The corresponding classification accuracies were derived by leave-one-  
4  
5 out cross validation and are listed in Table 3. Despite the extreme variation in concentrations  
6  
7 and RH levels within the two compared VOC groups, the six PAH-functionalized RN-  
8  
9 SWCNT chemiresistive sensors of array 1 achieved a good overall classification accuracy of  
10  
11 73.2%, using only one type of input variable ( $\Delta R/R_b$ ) from each sensor. As seen in the main  
12  
13 panel of Figure 5a, the nonpolar VOCs at the lowest RH level (5%) formed a tight cluster of  
14  
15 data points (full blue squares) that was well separated from the polar data points under 5% RH  
16  
17 (hollow red squares). The latter gave rise to two separate clusters corresponding to ethanol at  
18  
19 different concentrations spreading out to the upper right corner of the DFA map and all other  
20  
21 polar VOCs within a tight cluster on the upper left side of the nonpolar cluster. However, with  
22  
23 increasing RH background levels (40% RH and 80% RH) the clusters of polar and nonpolar  
24  
25 VOCs spread out and the data points gradually shifted from the right hemisphere of the DFA  
26  
27 map (*i.e.* positive values of CV1) to the left hemisphere (*i.e.* towards negative CV1 values).  
28  
29 The separate DFA models for the three RH levels further illustrate this trend (*see* side panels  
30  
31 of Figure 5a): The two clusters were very well defined and perfectly separated in an  
32  
33 atmosphere of 5% RH, spreading out and moving closer together while the RH level was  
34  
35 increased to 40% (classification accuracy of polar vs. nonpolar VOCs of 94%; *see* Table 3),  
36  
37 until the clusters started to overlap at 80% RH, slightly reducing the classification accuracy to  
38  
39 87%.  
40  
41  
42  
43  
44

45  
46 Array 2 of the six PAH-coated QCM mass-sensitive sensors achieved an even better  
47  
48 overall separation between the two groups of polar and nonpolar VOCs (*see* Figure 5b and  
49  
50 Table 3), with an excellent classification accuracy of 92% after cross validation. The separate  
51  
52 DFA analysis at a low background RH of 5% yielded two clusters that were less well-defined  
53  
54 and closer together than the corresponding clusters derived from the resistance responses of  
55  
56 array 1. Nevertheless, the intra-cluster spread of data points, the inter-cluster separation, the  
57  
58  
59  
60

1  
2  
3 classification accuracy and even the cluster position on the CV1 axis were hardly affected by  
4  
5 the strong increase in background RH between the partial models for 5%, 40% and 80% RH  
6  
7 represented in the side panels of Figure 5b. Hence, an array of the PAH-coated QCM sensors  
8  
9 such as array 2 could be used for the accurate classification of a VOC's polarity in an  
10  
11 atmosphere of extremely variable humidity.  
12

13  
14 Afterwards, we attempted a more detailed classification of the studied VOCs  
15  
16 according to the four different chemical groups that they belong to: alcohols, alkanes, ethers  
17  
18 and aromatics (*see* Table 2). Each group contained different VOCs at concentrations between  
19  
20  $p_a/p_o=0.05$  and  $p_a/p_o=0.2$  at variable background RH levels between 5% and 80%. The large  
21  
22 panel in Figure 6a displays a three-dimensional DFA model that was derived from the  
23  
24 resistance responses of array 1. As the figure shows, the clusters of the four chemical groups  
25  
26 were spread out and overlapped, when analyzing all the data at the different background RH  
27  
28 levels together, so that no separation between could be achieved. The classification accuracy  
29  
30 of the four groups was almost arbitrary after cross-validation (57%; *see* Table 3). This failure  
31  
32 resulted from the strong sensitivity of the PAH-functionalized RN-SWCNT sensors to the  
33  
34 humidity background. However, when analyzing the data separately at their three separate RH  
35  
36 levels, excellent classification results could be achieved. This can be seen in the three side  
37  
38 panels of Figure 6a, which demonstrate 2-dimensional DFA maps of the first two canonical  
39  
40 variables (CV1 and CV2). At 5% background RH, each chemical group formed a tight  
41  
42 cluster. The four clusters were well-separated from each other with a total classification  
43  
44 accuracy of 97% after cross-validation. Thereby the cluster of the polar alcohols was  
45  
46 especially far removed from the other three clusters of the nonpolar groups of alkanes, ethers  
47  
48 and aromatics. However, as the humidity background increased, we observed a pronounced  
49  
50 increase of the intra-cluster data spread within each chemical group and a decrease in inter-  
51  
52 cluster separation, leading to a decrease in classification accuracy of 94% for 40% RH to 80%  
53  
54  
55  
56  
57  
58  
59  
60

1  
2  
3 for 80% RH (*see* Table 3). The inability to classify all data gathered at varying RH levels  
4  
5 together stemmed mainly from a strong shift of the alcohol group (in red) to low values of  
6  
7 CV1 and a simultaneous shift of the alkanes group to higher values of CV1.  
8

9  
10 Figure 6b shows the same classification attempt according to the chemical groups,  
11  
12 using array 2 of 6 PAH-coated QCM sensors. Excellent and stable values were achieved for  
13  
14 the separation accuracy under each humidity background separately (all were above 94%; *see*  
15  
16 Table 3 and side panels of Figure 6b). Moreover, a very good overall classification was  
17  
18 obtained for all the data combined at variable RH levels between 5% and 80% (87.1%; *see*  
19  
20 Table 3). Each chemical group clustered separately, however, the mean distance of the  
21  
22 aromatic cluster from the other three chemical groups was most pronounced. This is in  
23  
24 agreement with the large responses of the separate QCM sensors to the aromatic compounds  
25  
26 and can be attributed to the similarity between the VOCs and the fused benzene rings in the  
27  
28 PAH cores.  
29  
30

31  
32 Subsequently, we attempted separating all the nine different VOC examined in this  
33  
34 study (*see* Table 2). An overall separation at RH levels between 5% and 80% failed both for  
35  
36 array 1 and array 2, since there were too many separation variables (*i.e.* VOCs) and not  
37  
38 enough predictor variables (*i.e.* sensing responses). However, we did succeed in separating  
39  
40 the clusters of the nine VOCs at each RH background level separately. Figure 7 summarizes  
41  
42 the DFA maps for the separate DFA models that were derived from the resistance responses  
43  
44 and the QCM mass uptakes. In agreement with our previous results, the best separation was  
45  
46 achieved, using the resistance responses of array 1 at 5% RH (97% accuracy; *see* Table 3).  
47  
48 The classification accuracy of array 1 decreased slightly and systematically to 89% for 80%  
49  
50 RH. In contrast, the accuracy of classification of the QCM sensor array increased from 78% at  
51  
52 5% RH to 94% at 80% RH. This behavior was expected and can be understood in terms of the  
53  
54 lack of compound separation of each separate QCM sensor at low RH and the pronounced  
55  
56  
57  
58  
59  
60

1  
2  
3 improvement thereof at increasing RH (*see* Figures 1&3). Also in agreement with the results  
4  
5 of the separate QCM sensors, the cluster of mesitylene could most easily be distinguished by  
6  
7 array 2, again due to the similarity between mesitylene and the fused benzene rings in the  
8  
9 PAH cores.  
10

11  
12 Finally, we divided array 1 and array 2 into two sub-arrays, in order to gain insight  
13  
14 into the role of the polarity of the PAH side-chains on their discrimination power between the  
15  
16 separate VOCs. The first sub-array consisted of the PAH-3,4&5 derivatives which possess  
17  
18 alternating hydrophobic alkyl side-chains and hydrophilic side-chains terminated with strong  
19  
20 polar functional substituents (ester and carboxyl). The second sub-array consisted of the PAH-  
21  
22 A,B&C having only hydrophobic alkyl side-chains (*see* Table 1). As described above, higher  
23  
24 resistance responses and mass uptakes upon exposure to both polar and nonpolar VOCs were  
25  
26 measured with the PAH-3,4&5 sensors than with the PAH-A,B&C sensors. Nevertheless the  
27  
28 higher responses did not yield better discrimination abilities. Table 4 summarizes the  
29  
30 classification accuracy for separate DFA models distinguishing between the 4 different polar  
31  
32 and the 5 different nonpolar VOCs under the different background RH levels of two sub-  
33  
34 arrays of PAH-functionalized RN-SWCNT chemiresistors and the corresponding two sub-  
35  
36 arrays of PAH-coated QCM sensors. Indeed, the sub-arrays based on PAH-A,B&C showed  
37  
38 superior discriminative ability both for nonpolar and for polar VOCs, despite their lower  
39  
40 sensing responses. The same observation was made for the chemiresistor array and the QCM  
41  
42 array. The PAH-3,4&5 derivatives performed reasonably well as chemiresistors, but were  
43  
44 clearly inferior to the PAH-A,B&C molecules as QCM sensing layers. Furthermore, in  
45  
46 agreement with the previous results, the classification accuracy for both QCM sub-arrays  
47  
48 improved with increasing background RH level, reaching their maximal values for 80% RH,  
49  
50 while the accuracy of classification with the chemiresistor-sub arrays showed a trend towards  
51  
52 lower values in more humid atmospheres. An exception to this rule was the separation of the 4  
53  
54  
55  
56  
57  
58  
59  
60

1  
2  
3 polar alcohols, which revealed a maximum at the intermediate RH value of 40% for both sub-  
4  
5 arrays. However, this result could very well be an arbitrary outlier. More systematic studies  
6  
7 with a larger number of independent measurements would be necessary to confirm these  
8  
9 results. The DFA method allows better valuation of the classification abilities of the two  
10  
11 arrays and improves their selectivity compared with the PCA results.  
12  
13

## 14 15 16 **SUMMARY AND CONCLUSION**

17  
18 We have presented a comparative study of the VOCs sensing performance of six custom-  
19  
20 designed PAH derivatives with different types of side chains as sensing elements in arrays of  
21  
22 chemiresistors and QCM sensors. The PAH derivatives provided good sensitivity and  
23  
24 selectivity towards different polar and nonpolar VOCs from the families of alcohols, alkanes,  
25  
26 ethers and aromatics under extremely varying humidity conditions (5-80% RH), while being  
27  
28 quite tolerant to large humidity variations. PAH derivatives having purely nonpolar side  
29  
30 chains had lower sensing responses than PAHs with alternating nonpolar and strongly polar  
31  
32 side chain termination, but nevertheless showed generally superior classification ability of  
33  
34 VOC polarity, chemical class and compound separation when grouped into arrays. Varying  
35  
36 humidity levels had opposite effects on arrays of QCM sensors and chemiresistors  
37  
38 incorporating the same PAH functional layers: While the resistance response was strongly  
39  
40 influenced by background humidity variations, the frequency response was relatively stable  
41  
42 over a wide range of humidity levels in the samples, from dry to almost fully humidified  
43  
44 atmospheres. We demonstrated that the chemiresistor arrays performed superior at controlled  
45  
46 RH levels, especially in dry atmospheres, whereas the QCM arrays were ideally suited for  
47  
48 applications under extremely variable background humidity.  
49  
50  
51  
52

53  
54 Note, however, that the frequency/mass measurements obtained in this work were  
55  
56 performed on pure PAH films, while the resistance measurements were performed on  
57  
58 PAH/RN-SWCNT bilayers. The reasoning behind facilitating relationships between the two  
59  
60



1  
2  
3 sets of measurements is that the resonant frequency/mass changes of RN-SWCNT-coated  
4  
5 QCM were between 4 to 15 times lower than the values measured by PAH-coated QCM. This  
6  
7 observation led us to the postulation that the RN-SWCNT layer has a minor effect on the  
8  
9 physical interaction with the organic vapors in relation to the PAH films which act as the  
10  
11 sensing layers with the sensors environment.  
12

13  
14 The results presented here could suggest guidelines governing the use of PAH  
15  
16 derivatives in different sensing platforms for a wide range of versatile real-world sensing  
17  
18 applications. An investigation the molecules' self-assembly and the resulting morphological  
19  
20 properties of the PAH layers would be of great value for mechanistically rationalizing the  
21  
22 sensing properties and optimizing PAH devices for sensing applications. A detailed  
23  
24 morphological study of the self-assembled layers presented in this report is underway and will  
25  
26 be published elsewhere. However, a true in-depth understanding of the sensing mechanism  
27  
28 that would allow flexible adaption of PAH-based sensing platforms requires additional  
29  
30 studies of different PAH molecules in which only one property is synthetically altered (*e.g.*  
31  
32 side chain length, functional end groups, and core geometry).  
33  
34  
35  
36  
37  
38  
39  
40  
41  
42  
43  
44  
45  
46  
47  
48  
49  
50  
51  
52  
53  
54  
55  
56  
57  
58  
59  
60

**ASSOCIATED CONTENT****Supporting Information**

Constituent sensors of the sensor arrays that were used in the current study; and response of PAH-QCM and PAH-4/SWCNT chemiresistor as a function of time at 5% RH. This material is available free of charge via the Internet at <http://pubs.acs.org>.

**AUTHOR INFORMATION**

Corresponding Author (H.H): [hhossam@tx.technion.ac.il](mailto:hhossam@tx.technion.ac.il)

**NOTES**

The authors declare no competing financial interest.

**ACKNOWLEDGMENTS**

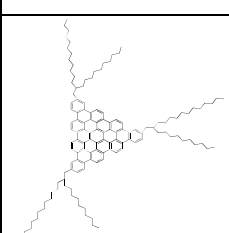
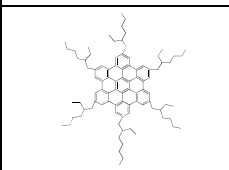
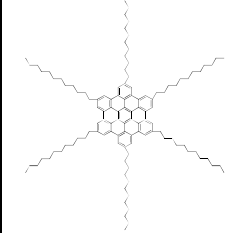
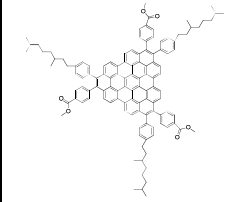
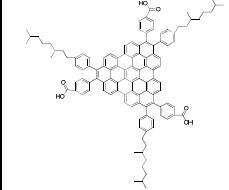
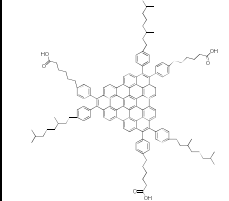
The research leading to these results has received funding from the FP7-Health Program under the LCAOS (Grant 258868), the FP7s ERC grant under DIAG-CANCER (Grant 256639), DFG Priority Program SPP 1355, ESF Project GOSPEL (Grant 09-EuroGRAPHENE-FP-001), EU Project GENIUS, and ERC grant on NANOGRAPH. We acknowledge Dr. Ulrike (Mirjam) Tisch, Ms. Alona Byan, Dr. Yair Paska and Ms. Lena Mintz (Technion - IIT) for fruitful discussions.

## REFERENCES

1. Konvalina, G.; Haick, H. *Acc. Chem. Res.* **2013**, DOI: 10.1021/ar400070m.
2. Broza, Y. Y.; Haick, H. *Nanomedicine (Future Medicine)* **2013**, *8*, 785-806.
3. Tisch, U.; Haick, H. *MRS Bull.* **2010**, *35*, 797-803.
4. Tisch, U.; Haick, H. *Rev. Chem. Eng.* **2010**, *26*, 171-179.
5. Roeck, F.; Barsan, N.; Weimar, U. *Chem. Rev.* **2008**, *108*, 705-725.
6. Houser, E. J.; Mlsna, T. E.; Nguyen, V. K.; Chung, R.; Mowery, R. L.; Andrew McGill, R. *Talanta* **2001**, *54*, 469-485.
7. Waggoner, P. S.; Craighead, H. G. *Lab Chip* **2007**, *7*, 1238-1255.
8. Di Pietrantonio, F.; Cannata, D.; Benetti, M.; Verona, E.; Varriale, A.; Staiano, M.; D'Auria, S. *Biosens. Bioelectron.* **2013**, *41*, 328-334.
9. Broza, Y.; Kremer, R.; Tisch, U.; Gevorkyan, A.; Shiban, A.; Best, L. A.; Haick, H. *Nanomedicine (New York, NY, US)* **2013**, *9*, 15-21.
10. Haick, H.; Hakim, M.; Patrascua, M.; Levenberg, C.; Shehada, N.; Nakhoul, F.; Abassi, Z. *ACS Nano* **2009**, *3*, 1258-1266.
11. Ionescu, R.; Broza, Y.; Shaltieli, H.; Sadeh, D.; Zilberman, Y.; Feng, X.; Glass-Marmor, L.; Lejbkowitz, I.; Müllen, K.; Miller, A.; Haick, H. *ACS Chem. Neurosci.* **2011**, *2*, 687-93.
12. Konvalina, G.; Haick, H. *ACS Appl. Mater. Interfaces* **2011**, *4*, 317-325.
13. Marom, O.; Nakhoul, F.; Tisch, U.; Shiban, A.; Abassi, Z.; Haick, H. *Nanomedicine (Future Medicine)* **2012**, *7*, 639-650.
14. Peled, N.; Barash, O.; Tisch, U.; Ionescu, R.; Broza, Y. Y.; Ilouze, M.; Mattei, J.; Bunn, P. A., Jr.; Hirsch, F. R.; Haick, H. *Nanomedicine (New York, NY, US)* **2013**.
15. Peled, N.; Hakim, M.; Bunn Jr, P. A.; Miller, Y. E.; Kennedy, T. C.; Mattei, J.; Mitchell, J. D.; Hirsch, F. R.; Haick, H. *J. Thorac. Oncol.* **2012**, *7*, 1528-1533.
16. Peled, N.; Ionescu, R.; Nol, P.; Barash, O.; McCollum, M.; VerCauteren, K.; Koslow, M.; Stahl, R.; Rhyan, J.; Haick, H. *Sens. Actuat. B* **2012**, *171-172*, 588-594.
17. Tisch, U.; Aluf, Y.; Ionescu, R.; Nakhleh, M.; Bassal, R.; Axelrod, N.; Robertman, D.; Tessler, Y.; Finberg, J. P. M.; Haick, H. *ACS Chem. Neurosci.* **2011**, *3*, 161-166.
18. Tisch, U.; Billan, S.; Ilouze, M.; Phillips, M.; Peled, N.; Haick, H. *CML-Lung Cancer* **2012**, *5*, 107-117.
19. Tisch, U.; Schlesinger, I.; Ionescu, R.; Nassar, M.; Axelrod, N.; Robertman, D.; Tessler, Y.; Azar, F.; Marmor, A.; Aharon-Peretz, J.; Haick, H. *Nanomedicine (Future Medicine)* **2012**, *8*, 43-56.
20. Xu, Z. Q.; Broza, Y. Y.; Ionescu, R.; Tisch, U.; Ding, L.; Liu, H.; Song, Q.; Pan, Y. Y.; Xiong, F. X.; Gu, K. S.; Sun, G. P.; Chen, Z. D.; Leja, M.; Haick, H. *Br. J. Cancer.* **2013**, *108*, 941-950.
21. Gutierrez-Osuna, R. *IEEE Sens. J.* **2002**, *2*, 189-202.
22. Marco, S.; Gutiérrez-Gálvez, A. *IEEE Sens. J.* **2012**, *12*, 3189-3214.
23. Vlachos, D. S.; Skafidas, P. D.; Avaritsiotis, J. N. *Sens. Actuat. B* **1995**, *25*, 491-494.
24. Barash, O.; Peled, N.; Tisch, U.; Jr., B. P. A.; Hirsch, F. R.; Haick, H. *Nanomedicine (New York, NY, US)* **2012**, *8*, 580-589.
25. Krasteva, N.; Fogel, Y.; Bauer, R. E.; Müllen, K.; Joseph, Y.; Matsuzawa, N.; Yasuda, A.; Vossmeier, T. *Adv. Funct. Mater.* **2007**, *17*, 881-888.
26. Li, B.; Santhanam, S.; Schultz, L.; Jeffries-El, M.; Iovu, M.; Sauvé, G.; Cooper, J.; Zhang, R.; Revelli, J.; Kusne, A.; Snyder, J.; Kowalewski, T.; Weiss, L.; McCullough, R.; Fedder, G.; Lambeth, D. *Sens. Actuat. B* **2007**, *123*, 651-660.
27. Peng, H.; Soeller, C.; Vigar, N.; Caprio, V.; Travas-Sejdic, J. *Biosens. Bioelectron.* **2007**, *22*, 1868-1873.
28. Regmi, B.; Monk, J.; El-Zahab, B.; Das, S.; Hung, F.; Hayes, D.; Warner, I. *J. Mater. Chem.* **2012**, *22*, 13732-13741.
29. Segev-Bar, M.; Shuster, G.; Haick, H. *J. Phys. Chem. C* **2012**, *116*, 15361-15368.
30. Shen, G.; Chen, P. C.; Ryu, K.; Zhou, C. *J. Mater. Chem.* **2009**, *19*, 828-39.
31. Sysoev, V. V.; Strelcov, E.; Sommer, M.; Bruns, M.; Kiselev, I.; Habicht, W.; Kar, S.; Gregoratti, L.; Kiskinova, M.; Kolmakov, A. *ACS Nano* **2010**, *4*, 4487-4494.
32. Wang, J. *Electroanalysis* **2005**, *17*, 7-14.
33. Zilberman, Y.; Ionescu, R.; Feng, X.; Müllen, K.; Haick, H. *ACS Nano* **2011**, *5*, 6743-6753.

- 1  
2  
3 34. Bachar, N.; Mintz, L.; Zilberman, Y.; Ionescu, R.; Feng, X.; Müllen, K.; Haick, H. *ACS Appl. Mater. Interfaces* **2012**, *4*, 4960-65.
- 4  
5 35. Xu, X.; Cang, H.; Li, C.; Zhao, Z.; Li, H. *Talanta* **2009**, *78*, 711-716.
- 6 36. Shin, H.; Yoo, S.; Kim, J.; Kwon, Y. *Mol. Cryst. Liq. Cryst. Sci. Technol. A* **1997**, *295*, 137-140.
- 7 37. Amal, H.; Ding, L.; Liu, B. B.; Tisch, U.; Xu, Z. Q.; Shi, D. Y.; Zhao, Y.; Chen, J.; Sun, R. X.; Liu, H.; Ye, S. L.; Tang, Z. Y.; Haick, H. *Int. J. Nanomed.* **2012**, *7*, 4135-4146.
- 8  
9 38. Bayn, A.; Feng, X.; Müllen, K.; Haick, H. *ACS Appl. Mater. Interfaces* **2013**, *5*, 3431-3440.
- 10 39. Zilberman, Y.; Tisch, U.; Pisula, W.; Feng, X.; Mullen, K.; Haick, H. *Langmuir* **2009**, *25*, 5411-5416.
- 11  
12 40. Zilberman, Y.; Tisch, U.; Shuster, G.; Pisula, W.; Feng, X.; Mullen, K.; Haick, H. *Adv. Mater.* **2010**, *22*, 4317-4320.
- 13  
14 41. Feng, X.; Liu, M.; Pisula, W.; Takase, M.; Li, J.; Müllen, K. *Adv. Mater.* **2008**, *20*, 2684-2689.
- 15 42. Kastler, M.; Pisula, W.; Wasserfallen, D.; Pakula, T.; Müllen, K. *J. Am. Chem. Soc.* **2005**, *127*, 4286-4296.
- 16  
17 43. Feng, X.; Pisula, W.; Zhi, L.; Takase, M.; Müllen, K. *Angew. Chem. Int. Ed.* **2008**, *47*, 1703-1706.
- 18 44. Feng, X.; Pisula, W.; Kudernac, T.; Wu, D.; Zhi, L.; De Feyter, S.; Müllen, K. *J. Am. Chem. Soc.* **2009**, *131*, 4439-4448.
- 19  
20 45. Feng, X. L.; Marcon, V.; Pisula, W.; Hansen, M. R.; Kirkpatrick, J.; Andrienko, D.; Kremer, K.; Müllen, K. *Nature Mater.* **2009**, *8*, 421-426.
- 21  
22 46. Hirschberg, J. H.; Brunsveld, L.; Ramzi, A.; Vekemans, J. A.; Sijbesma, R. P.; Meijer, E. W. *Nature* **2000**, *407*, 167-170.
- 23  
24 47. Lower concentrations than  $p_a/p_o=0.05$  are not stable along the time of the experiment. Higher concentrations than  $p_a/p_o=0.2$  might be associated with condensation of the VOCs on the surface of the sensors (*cf.* ref. 53). To eliminate these potential problems from our **comparative** study, the concentration in the current study was limited to  $p_a/p_o=0.05$ .
- 25  
26 48. These three RH values are representative examples for low (*e.g.*, 5%) RH levels that exist usually in closed and well-controlled systems, medium (*e.g.*, 40%) RH values that exist usually in the atmosphere/environment, and for high (*e.g.*, 80%) RH values that exist in the environment or in diagnostically-related clinical samples, such as exhaled breath.
- 27  
28 49. Brereton, R. G., *Chemometrics, Application of Mathematics and Statistics to Laboratory Systems*. Ellis Horwood: Chichester, UK, 1990.
- 29  
30 50. Charlesworth, M.; Partridge, C.; Garrard, N. *J. Phys. Chem.* **1993**, *97*, 5418-5423.
- 31  
32 51. Bissell, R. A.; Persaud, K. C.; Travers, P. *Phys. Chem. Chem. Phys.* **2002**, *4*, 3482-3490.
- 33  
34 52. Topart, P.; Josowicz, M. *J. Phys. Chem.* **1992**, *96*, 8662-8666.
- 35  
36 53. Paska, Y.; Stelzner, T.; Assad, O.; Tisch, U.; Christiansen, S.; Haick, H. *ACS Nano* **2011**, *6*, 335-345.
- 37  
38 54. Paska, Y.; Stelzner, T.; Christiansen, S.; Haick, H. *ACS Nano* **2011**, *5*, 5620-5626.
- 39  
40 55. Blackwood, D.; Josowicz, M. *J. Phys. Chem.* **1991**, *95*, 493-502.
- 41  
42 56. Sherrington, D.; Taskinen, K. *Chem. Soc. Rev.* **2001**, *30*, 83-93.
- 43  
44 57. Hunter, C.; Lawson, K.; Perkins, J.; Urch, C. *J. Chem. Soc.* **2001**, *5*, 651-669.
- 45  
46 58. Schon, J. H.; Kloc, C.; Dodabalapur, A.; Crone, B. *Appl. Phys. Lett.* **2001**, *79*, 3965-3967.
- 47  
48 59. Haynes, W. M., *CRC Handbook of Chemistry and Physics 91st ed.* CRC Press: Boulder, CO, 2010.
- 49  
50  
51  
52  
53  
54  
55  
56  
57  
58  
59  
60

**Table 1:** Structural properties of the PAH derivatives

name	core shape	no. of C atoms in the core	side-group termination	side-group polarity	structure
PAH-A	triangular	60	branched alkyl chain	nonpolar	
PAH-B	hexagonal	42	branched alkyl chain		
PAH-C	hexagonal	42	alkyl chain		
PAH-3	semi-triangular	48	alternating ester (methyl) & branched alkyl chain	alternating strongly polar and nonpolar termination	
PAH-4	semi-triangular	48	alternating carboxyl & branched alkyl chain		
PAH-5	semi-triangular	48	alternating carboxyl & branched alkyl chain		

**Table 2:** Physical properties of the VOCs used for the exposure experiments (taken from ref. 59)

VOC	polarity	chemical family	formula	molecular mass (g·mol <sup>-1</sup> )	vapor pressure (kpa@20°C)	dipole moment (debye)	dielectric constant	density (g·cm <sup>-3</sup> )
hexane	nonpolar	alkanes	CH <sub>3</sub> (CH <sub>2</sub> ) <sub>4</sub> CH <sub>3</sub>	86.23	17.6	0	1.89	0.655
octane			CH <sub>3</sub> (CH <sub>2</sub> ) <sub>6</sub> CH <sub>3</sub>	114.2	1.47	0	1.94	0.703
decane			CH <sub>3</sub> (CH <sub>2</sub> ) <sub>8</sub> CH <sub>3</sub>	142.3	1.58	0	1.98	0.730
<i>di</i> -butylether		ether	[CH <sub>3</sub> (CH <sub>2</sub> ) <sub>3</sub> ] <sub>2</sub> O	130.2	0.640	0	3.1	0.769
mesitylene		aromatic	C <sub>6</sub> H <sub>3</sub> (CH <sub>3</sub> ) <sub>3</sub>	120.2	0.230	0	2.4	0.864
ethanol	polar	alcohols	CH <sub>3</sub> CH <sub>2</sub> -OH	46.07	5.95	1.69	24.3	0.789
1-hexanol			CH <sub>3</sub> (CH <sub>2</sub> ) <sub>5</sub> -OH	102.2	0.133	1.80	13.3	0.813
1-octanol			CH <sub>3</sub> (CH <sub>2</sub> ) <sub>7</sub> -OH	130.2	0.114	1.76	10.3	0.824
1-decanol			CH <sub>3</sub> (CH <sub>2</sub> ) <sub>9</sub> -OH	158.3	0.015	1.68	7.93	0.830
water		water	H <sub>2</sub> O	18.01	2.34	1.85	80.4	1.000

**Table 3:** Classification accuracy (%) derived by leave-one-out cross validation for the DFA models represented in Figures 5-7.

DFA model	sensors array	classification accuracy (%)			
		5% RH	40% RH	80% RH	all data
differentiating between a group of polar and a group of nonpolar VOCs ( <i>cf.</i> Figure 5)	array 1: PAH-functionalized RN-SWCNTs chemiresistors	100	94.4	86.9	73.2
	array 2: PAH-coated QCM	100	100	94.4	91.6
differentiating between different chemical families of alcohols, alkanes, ethers and aromatic ( <i>cf.</i> Figure 6)	array 1: PAH-functionalized RN-SWCNTs chemiresistors	97.2	94.4	80.6	56.6
	array 2: PAH-coated QCM	94.4	98.1	94.4	87.1
differentiating between the separate VOCs (decanol, octanol, hexanol, ethanol, decane, octane, hexane, dibutylether and mesitylene; <i>cf.</i> Figure 7)	array 1 PAH-functionalized RN-SWCNTs chemiresistors	97.2	94.4	88.9	arbitrary results
	array 2: PAH-coated QCM	77.8	91.6	94.4	

**Table 4:** Discrimination accuracy between the four different polar VOCs and five different nonpolar VOCs under various background RH levels of two sub-arrays of PAH-functionalized RN-SWCNT chemiresistors (PAH-3,4&5, which stands for alternating strongly polar and nonpolar side chains; and PAH-A,B&C that stands for nonpolar side chains alone) and the corresponding two sub-arrays of PAH-coated QCM sensors.

		PAH-functionalized RN-SWCNTs		PAH-coated QCM	
group	humidity background	PAH-3,4&5	PAH-A,B&C	PAH-3,4&5	PAH-A,B&C
nonpolar VOCs	5% RH	90	100	55	65
	40% RH	70	95	60	75
	80% RH	70	85	75	90
polar VOCs	5% RH	87.5	87.5	50	87.5
	40% RH	93.8	100	68.8	87.5
	80% RH	87.5	93.8	75	100

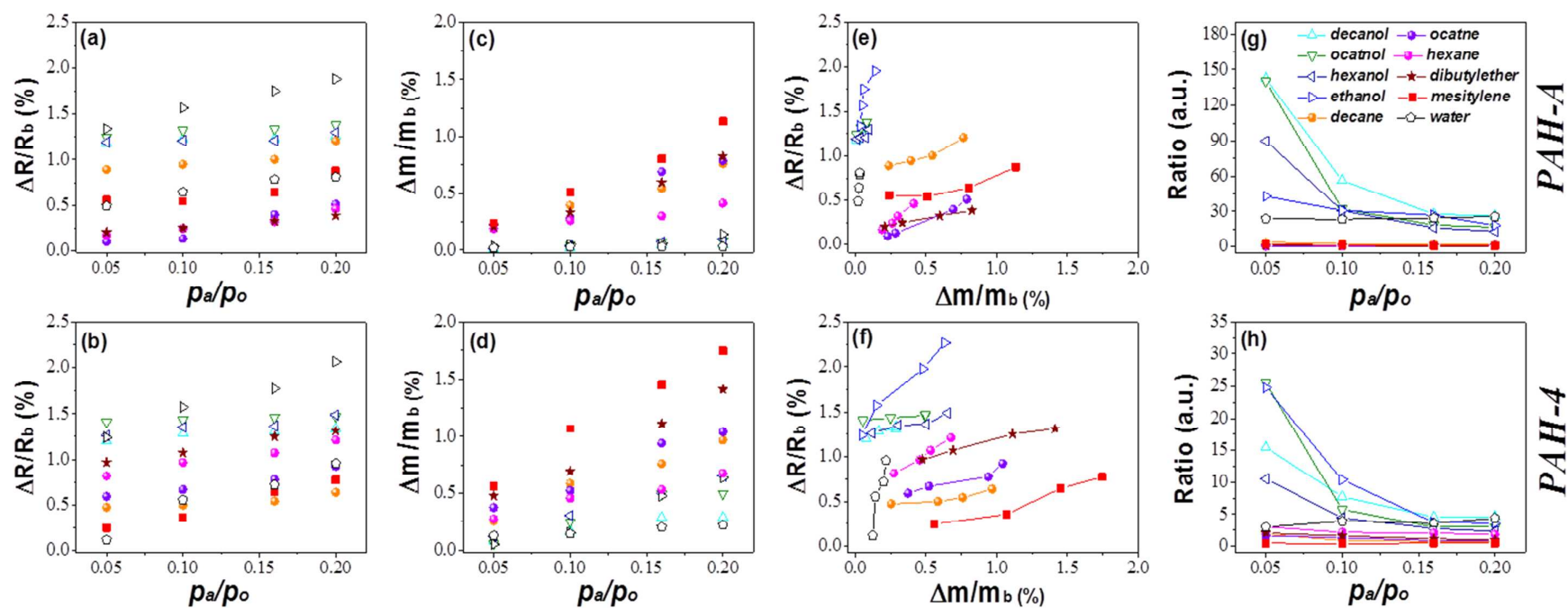


**Figure 1:** Plots of relative electrical resistance changes ( $\Delta R/R_b$ ) vs. VOC concentration ( $p_a/p_o$ ) for (a) PAH-A, as a representative example for the group of PAH derivatives with only hydrophobic alkyl side-chains; and (b) PAH-4, as a representative example for the group of the PAH derivatives with alternating hydrophobic alkyl side-chains and hydrophilic side-chains. Plots of relative mass changes ( $\Delta m/m_b$ ) vs. VOC concentration for (c) PAH-A; and (d) PAH-4. Plots of  $\Delta R/R_b$  vs.  $\Delta m/m_b$  for (e) PAH-A; and (f) PAH-4. Plots of the ratio between  $\Delta R/R_b$  and the  $\Delta m/m_b$  vs. VOC concentration ( $p_a/p_o$ ) for (g) PAH-A; and (h) PAH-4. All data presented in the plots were obtained under 5% RH background. The error bars of the measurements are smaller than the symbol size.



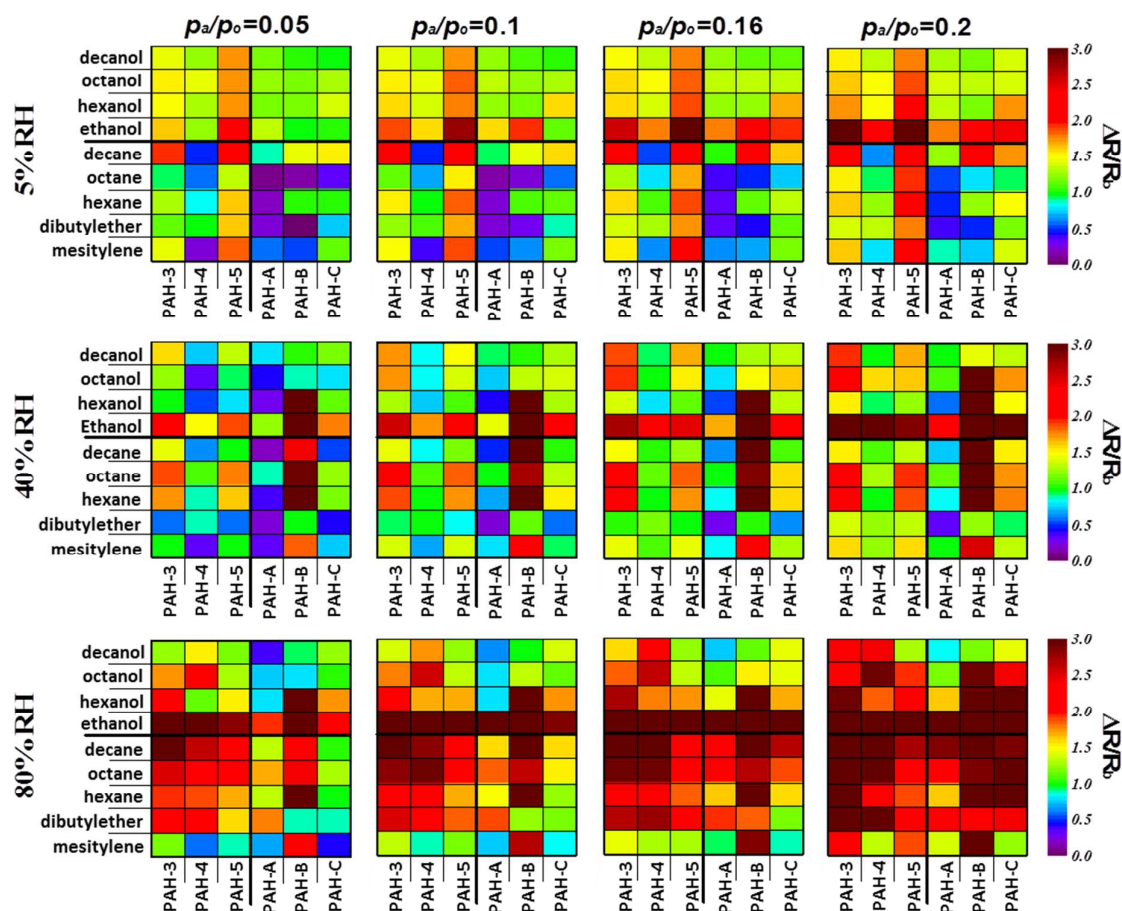


**Figure 2:** Heat-maps of the relative electrical resistance changes ( $\Delta R/R_b$ ) of the six constituent PAH-functionalized RN-SWCNT chemiresistors in array 1 upon exposure to 4 polar VOCs and 5 nonpolar VOCs, at four VOC concentrations (columns):  $p_a/p_o=0.05$ , 0.1, 0.16, and 0.2; under three levels of background humidity (rows): RH = 5%, 40% and 80%. The signal strength is represented by the differences in color.

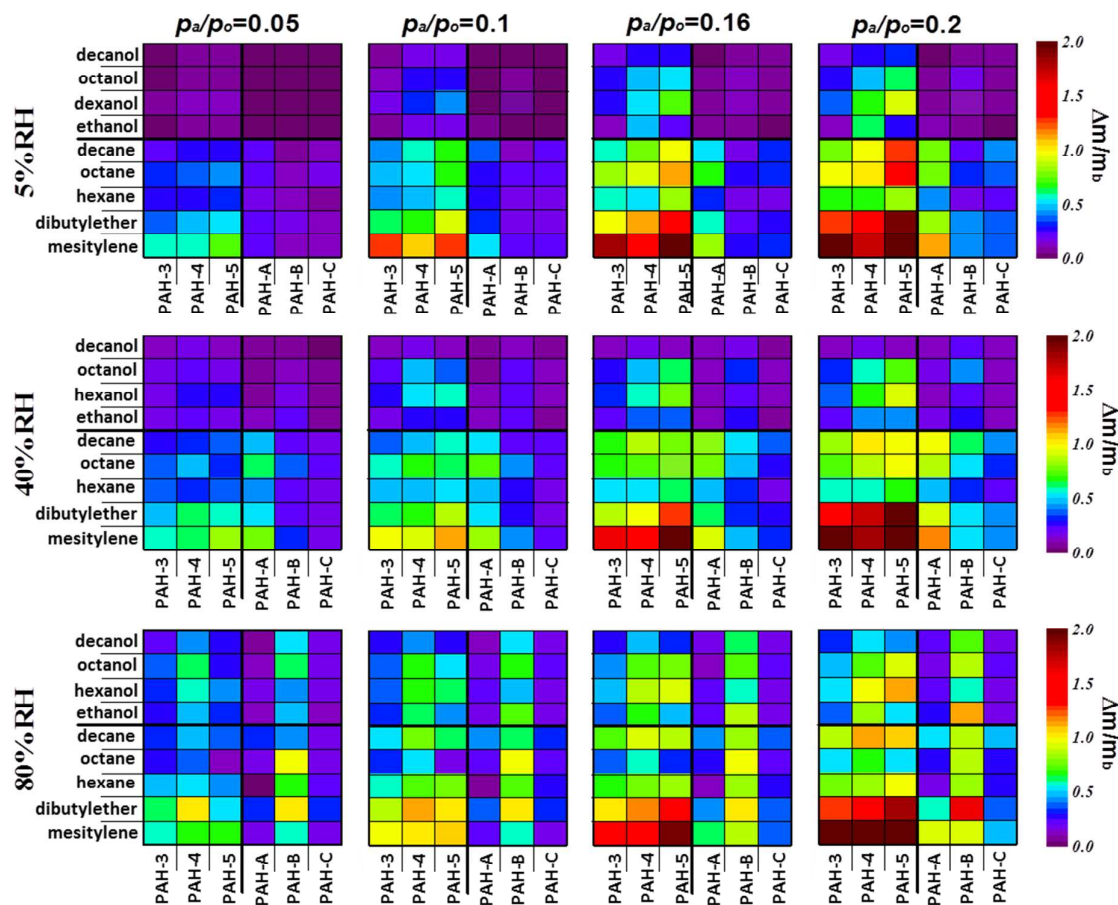


**Figure 3:** Heat-maps of the relative mass changes ( $\Delta m/m_b$ ) of the six constituent PAH-coated QCM sensors in array 2 upon exposure to 4 polar VOCs and 5 nonpolar VOCs, at four VOC concentrations (columns):  $p_a/p_o=0.05, 0.1, 0.16, \text{ and } 0.2$ ; under three levels of background humidity (rows): RH = 5%, 40% and 80%. The signal strength is represented by the differences in color.

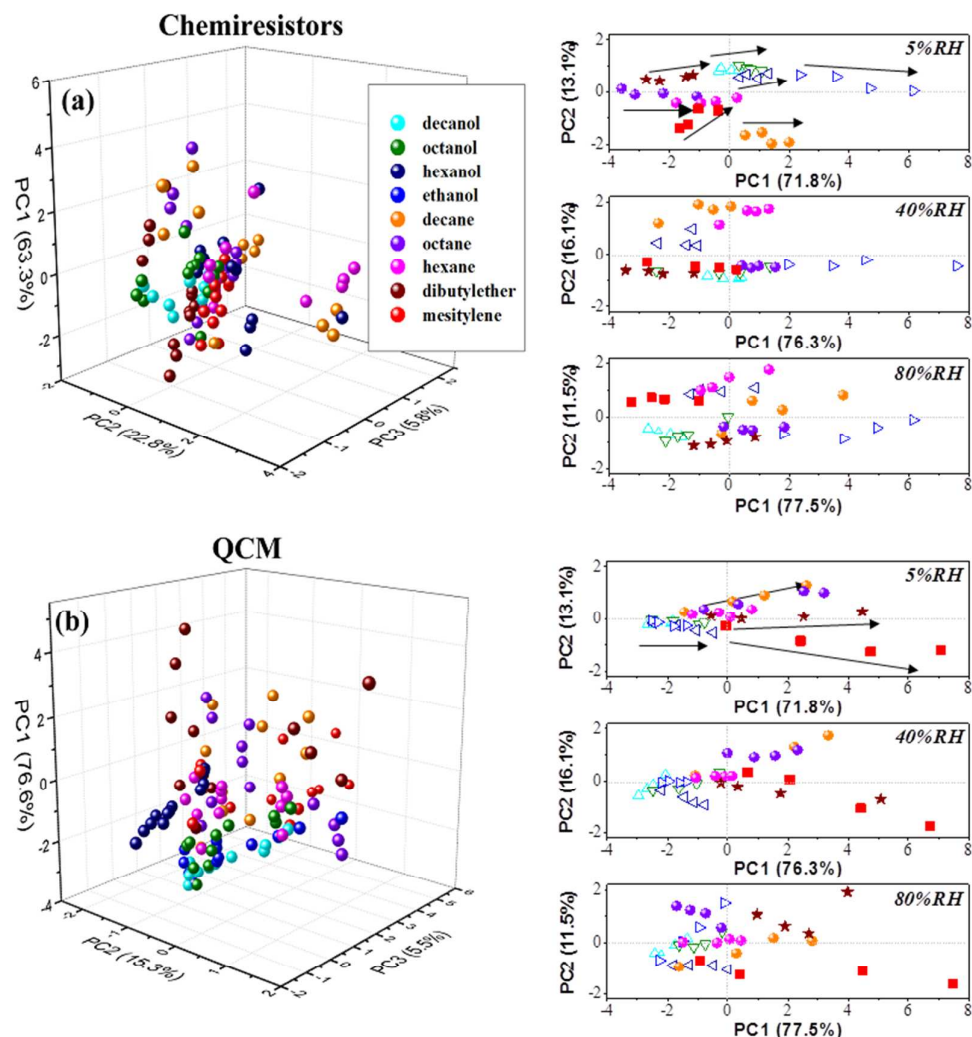


**Figure 4:** PCA plots separating between the different VOCs examined in the study (decanol, octanol, hexanol, ethanol, decane, octane, hexane, dibutylether and mesitylene,  $p_a/p_o = 0.05-0.2$ , RH = 5-80%) using **(a)** the complete array 1 of six PAH-functionalized RN-SWCNT chemiresistive sensors, and **(b)** the complete array 2 of six PAH-coated QCM mass-sensitive sensors. The side panels show the PCA plots of separate analysis at the three RH levels. The arrows direction indicate an increasing concentration from  $p_a/p_o=0.05$  to  $p_a/p_o=0.2$ .

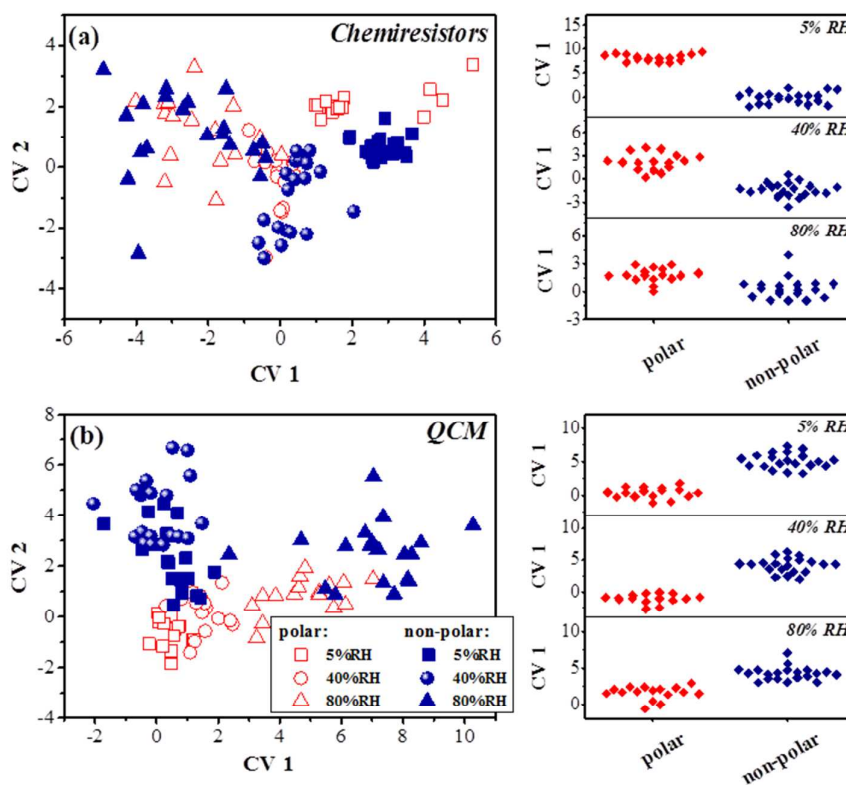


**Figure 5:** DFA results differentiating between the group of polar VOCs and the group of nonpolar VOCs (*cf.* Table 1) at different concentrations ( $p_a/p_o = 0.05, 0.1, 0.16, 0.2$ ) under 5%, 40% and 80% RH using (a) the complete array 1 of six PAH-functionalized RN-SWCNT chemiresistive sensors, and (b) the complete array 2 of six PAH-coated QCM mass-sensitive sensors. The side panels show the binary DFA maps of separate analysis at the three RH levels.

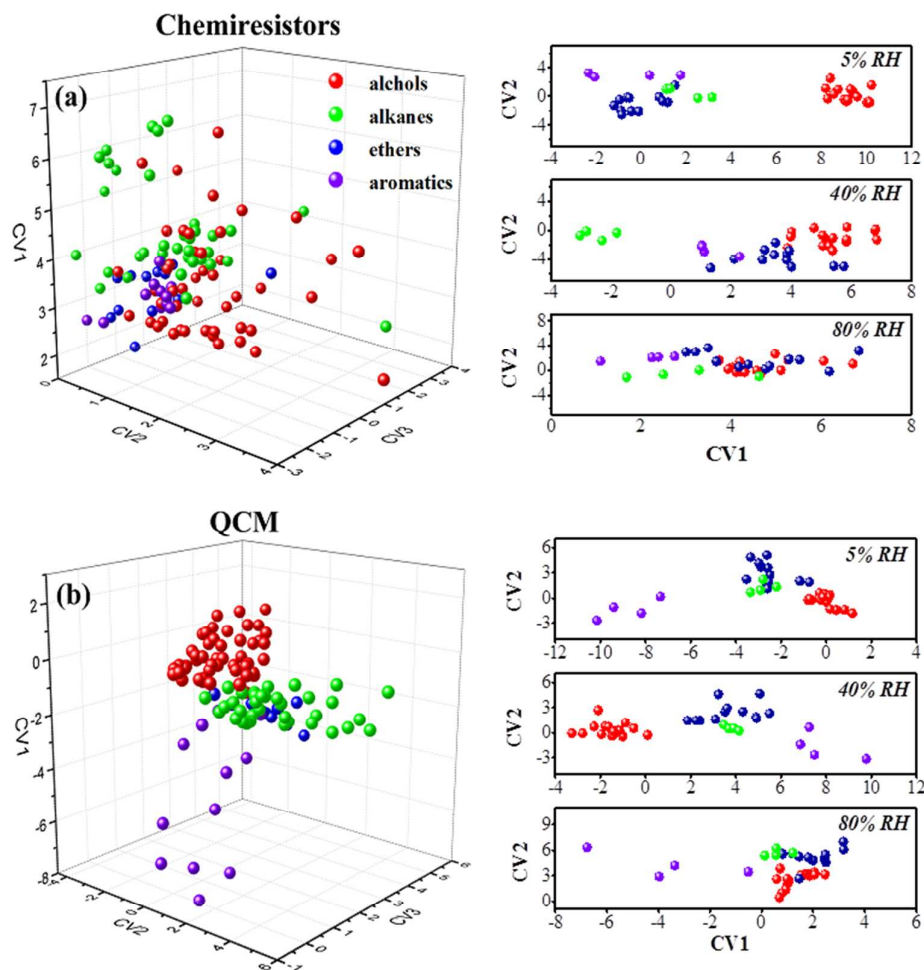


**Figure 6:** DFA results differentiating between different chemical families of alcohols, alkanes, ethers and aromatics (*cf.* Table 1) at different concentrations ( $p_a/p_o = 0.05, 0.1, 0.16, 0.2$ ) under 5%, 40% and 80% RH using (a) the complete array 1 of six PAH-functionalized RN-SWCNT chemiresistor, and (b) the complete array 2 of six PAH-coated QCM mass-sensitive sensors. The side panels show the DFA maps of separate analysis at the three RH levels.

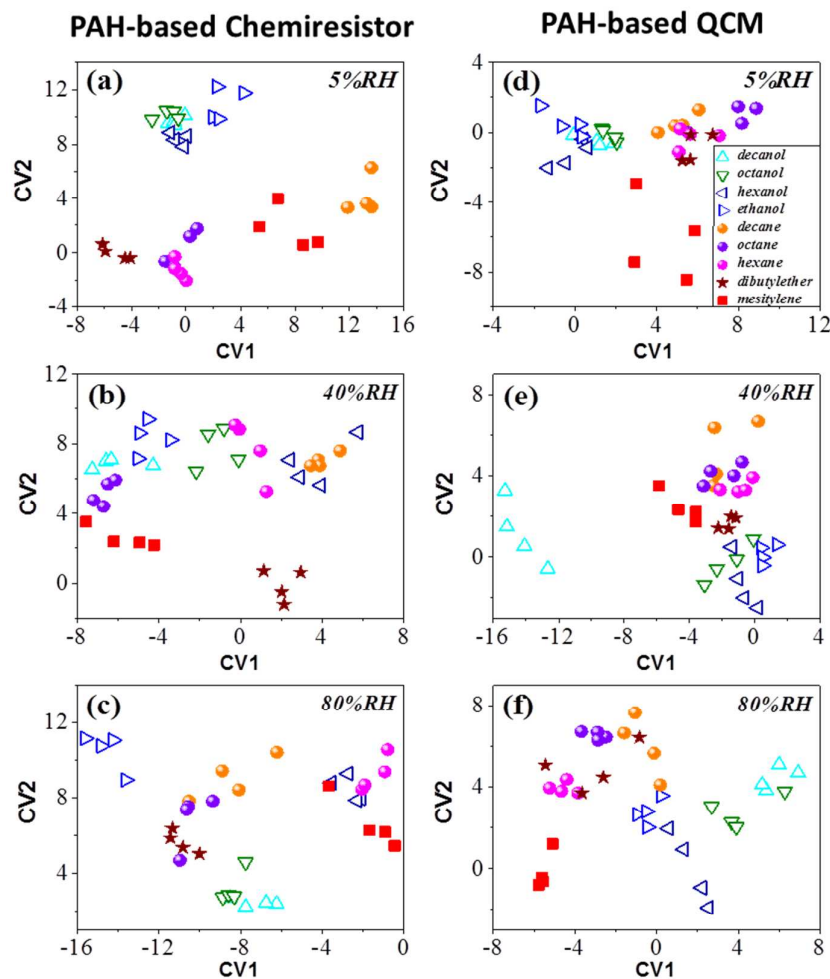


**Figure 7:** DFA maps of models separating between the different VOCs examined in the study under humidity levels of (a) 5%, (b) 40% and (c) 80% RH using a complete array of 6 PAH-functionalized RN-SWCNT chemiresistor. DFA results of the data measured for the same VOCs under (d) 5%, (e) 40% and (f) 80% RH using a complete array of six PAH-coated QCM mass-sensitive sensors.

1  
2  
3 **TOC Figure:**  
4  
5  
6  
7  
8  
9  
10  
11  
12  
13  
14  
15  
16  
17  
18  
19  
20  
21  
22  
23  
24  
25  
26  
27  
28  
29  
30  
31  
32  
33  
34  
35  
36  
37  
38  
39  
40  
41  
42  
43  
44  
45  
46  
47  
48  
49  
50  
51  
52  
53  
54  
55  
56  
57  
58  
59  
60

